Experimental investigation and probabilistic modelling of the load–displacement behaviour of steel-to-timber joints with self-tapping

Citation for the original published paper (version of record):
Caprio, D., Jockwer, R. (2025). Experimental investigation and probabilistic modelling of the load–displacement behaviour of
steel-to-timber joints with self-tapping screws. Construction and Building Materials, 489.
http://dx.doi.org/10.1016/j.conbuildmat.2025.141970

Construction and Building Materials 489 (2025) 141970

Contents lists available at ScienceDirect

Construction and Building Materials

journal homepage: www.elsevier.com/locate/conbuildmat

Experimental investigation and probabilistic modelling of the load–displacement behaviour of steel-to-timber joints with self-tapping screws

Dorotea Caprio [a,*], Robert Jockwer [b]

[a] Division of Structural Engineering, Department of Architecture and Civil Engineering (ACE), Chalmers University of Technology, Sven Hultins gata 6, 412 96 Gothenburg, Sweden

[b] Chair of Timber Engineering, TUD Dresden University of Technology, George-Bähr-Str.1, 01069 Dresden, Germany

ARTICLE INFO

Keywords:
Self-tapping screws
Steel-to-timber joints
Asymmetric test set-up
Variability
Empirical-probabilistic model
Slip-modulus
Ductility

ABSTRACT

The load–displacement behaviour of timber joints is nonlinear, yet simplistic assumptions are often made in the design phase, leading to an idealized elastic-perfectly plastic representation of their response. This highlights the need for more refined models to accurately describe their mechanical behaviour. An example of modern timber joints is represented by steel-to-timber joints that employ laterally and axially loaded self-tapping screws, common in large timber structures. In this paper, first, the impact of different parameters of influence: the test set-up, the screw length, the friction, the torque, the load-to-screw axis angle, and moisture cycling on the load–displacement of joints with screws under applied lateral-tension load, was studied. Then, 10 to 20 tests were performed for every load-to-screw axis angle, for a total of 60 tests, to describe the shape and the variability of the load–displacement curve. Based on this experimental data, an empirical-probabilistic model using the Richard-Abbott analytical expression for describing the load–displacement curve was developed, and the model parameters were determined. A comparison of slip-modulus values at ultimate limit state derived from the empirical-probabilistic model with values prescribed by Eurocode 5 suggested that the current definition may be inadequate for steel-to-timber joints with screws. Beyond this contribution scope, the empirical-probabilistic model constitutes an input for multi-fastener joint models, which can subsequently be incorporated into the reliability analysis of timber structures.

1. Introduction

1.1. Joints with screws

Joints with self-tapping screws do not count only on the embedment properties of the system screw-timber, but also, if placed and loaded at an angle to the shear plane, on the withdrawal properties of the screws. Consequently, these joints mechanical behaviour is characterized by higher elastic slip-modulus and load-carrying capacity than only laterally loaded fasteners. For this characteristic, joints with screws are used in multiple applications: beam-to-column and beam-to-beam joints, floor-to-floor, wall-to-wall, floor-to-wall, and beam-to-beam connections in CLT or hybrid structures [1–3]. Unfortunately, this remarkable progress in construction technology is not adequately reflected in the definition of design rules for timber joints in Eurocode 5 (EC5) [4], which often involve an over-simplification of the joint mechanical behaviour. So far, only the characteristic load-carrying capacity and the mean slip-modulus at the serviceability limit state (SLS) are specified in EC5. A simple reduction of the elastic slip-modulus is implemented to take the non-linear behaviour into account at the ultimate limit state (ULS). No information about the ductility of these joints is given, which may be relevant, particularly for seismic or robustness purposes. Moreover, the entire load–displacement curve and its variability are needed to perform reliability analysis.

1.2. Tests in literature

Several past studies investigated the mechanical behaviour of joints with screws. These studies focused on the axial tension behaviour [5–14], others on the combined action of lateral and tension loading on the screws, both on timber-to-timber and steel-to-timber joints [15–19]. Another study investigated the impact of the interlayers (such as insulation) on the mechanical behaviour of joints [20]. The test set-up used include push-out and pull-out tests in symmetrically loaded timber

* Corresponding author.
E-mail addresses: dorotea.caprio@chalmers.se (D. Caprio), robert.jockwer@tu-dresden.de (R. Jockwer).

https://doi.org/10.1016/j.conbuildmat.2025.141970
Received 20 March 2025; Received in revised form 16 May 2025; Accepted 24 May 2025
Available online 20 June 2025

joint configurations with joints on both sides. In the following, the test series from the literature most relevant to this study are elaborated. The study conducted in [5] showed that the arrangement of lamellae in glulam and CLT affects the withdrawal capacity of self-tapping screws; additionally, faster loading rates increased capacity, whereas higher moisture levels reduced it. In [15], timber-to-timber joints were tested with varying distances among the screws and load-to-screw axis angles (45°, 60°, 75°, 90°). In some configurations, the screws were subjected to the combined action of lateral and tension load, and in others to the combined action of lateral and compression load. The load-to-screw axis angle was varied, and it was found that it had a big impact on the shape of the load–displacement curves. In particular, smaller angles resulted in a larger elastic slip-modulus, higher load-carrying capacity, and less ductility. In [16], steel-to-timber joints were tested, and the load-to-screw axis angle, the number of screws in a row, the number of rows, and the coefficient of friction were varied. At least 10 repetitions for each configuration were tested. The focus was mainly on the effect of the number of fasteners in a row. The aim was to quantify the effective number of fasteners if the prescribed distances are adopted. In [17], timber-to-timber joints with inclined and not inclined screws were tested under tension load and a combination of lateral and tension load. The impact of timber density on the load–displacement curves and their variability was assessed for different load-to-screw axis angles (45°, 60°, 90°). The joints with higher density were characterized by larger elastic slip-modulus, load-carrying capacity and ductility. In [21], tests on laterally loaded and a combination of lateral and tension load on joints with screws were carried out with and without the presence of a soundproof layer. The main outcome was that the soundproof layer had a larger impact on elastic slip-modulus than on the load-carrying capacity and that this was true in particular for joints with inclined screws.

In these experimental campaigns, the first insights into the variability of the load-deformation behaviour of screw joints can be found. However, open questions remain regarding the impact of other influence parameters, such as friction, torque, washer, and moisture cycling. Moreover, the mechanical behaviour of a screw tested in symmetric configurations is affected by the presence of the other screw, which results in the re-distribution of forces and allows for alternative load paths. In this study asymmetric test set-up where single screws were compared with symmetric test-set up. Using an asymmetric test set-up allowed to isolate the relevant parameters of influence on the load-deformation behaviour.

1.3. Models in literature

In EC5 the load-carrying capacity of a multi-fastener joint is derived directly from the capacity of a single fastener. The load-carrying capacity of a single fastener is calculated according to the European Yield Model, which uses two key parameters obtained from single-fastener tests: the embedment capacity and the bending yield moment of a fastener. An empirically derived "effective number" factor is then applied to the single fastener capacity to obtain the capacity of a group of fasteners, accounting for spacing and uneven load sharing (originally proposed by Jorissen [22]).

Recent research has extended beyond load-carrying capacity predictions to capture the full load–displacement curves of multi-fastener and single fastener joints. These approaches include: empirical, mechanical and semi-analytical models.

The empirical models are based on regression over the observed data. Regression uses analytical expressions such as polynomial, rational, or exponential functions or analytical models such as Foschi or Richard-Abbott, fitted directly to experimental curves [23,24]. While functions do not possess a physical interpretation of the parameters, analytical models can describe the load–displacement behaviour in the function of physically meaningful parameters. A detailed summary of different functions used to describe the load-deformation behaviour of joints is given in [23,24]. Functions and analytical models were, for example, used in [21,23–26]. In [25], a multi-step approach for the parametrization of the nonlinear load–displacement was applied to describe the embedment behaviour of single fastener as a function of load-to-grain angle. The authors showed the suitability of the three-step approach through a regression analysis of the load–displacement curve using a large experimental database of embedment tests. In [23] a rational function was developed to describe the non-linear behaviour of hold-downs with screws and then used as input for a pushover analysis. In [26] the load–displacement behaviour of single, axially screw positioned in the narrow face of CLT and failing in withdrawal was investigated. An empirical probabilistic model was formulated using analytical models [27].

Mechanical models include 3D or 2D finite element models. In 3D solid finite element models, the interaction between the fastener and the surrounding wood is modelled by surface-to-surface contacts with a penalty formulation. 3D models for timber joints with screws were developed, for example, in [28], where the model of timber-to-timber joints and composite beams with screws was validated against experimental results from the state-of-art. Material properties and cohesive interface damage contacts were properly calibrated to take into account possible local effects. These models can reproduce complex stress fields, but they are limited by the often occurring convergence criteria due to local stress concentration [28,29]. In 2D finite element models, the fastener is replaced by a spring that can be linear or non-linear, whose load–displacement is derived from experimental results or empirical models [23,25]. Another mechanical model is represented by the beam-on-foundation model, which can be used to predict the entire load–displacement curve of a single fastener joint. In this case, the fastener is modelled by a beam element and the interaction with the surrounding timber is modelled by linear or non-linear springs. The springs can be placed parallel and perpendicular to grain or parallel and perpendicular to the screw axis [20]. The beam-on-foundation model was used, for example, in [20] to model steel-to-timber and timber-to-timber joints a with single screw. Due to the interaction between the axial and the lateral behaviour, the authors highlighted how these models might not accurately predict the behaviour of joints with a screw.

Semi-analytical joint models represent a compromise between accuracy and computational time. These models are based on kinematic and equilibrium considerations, assuming the timber member as rigid and modelling the fastener behaviour with a nonlinear spring. The output is the full load–displacement curve. This semi-analytical approach was successfully applied previously by [30], to obtain the load–displacement curve of moment-resisting joints with dowels and slotted-in plates.

So far, the majority of existing models lack the probabilistic description of the mechanical behaviour of inclined screws subjected to the combined lateral and axial tension load. For this reason, an empirical probabilistic model about inclined screws varying the load-to-screw axis angle was developed in this study. This model can be later used into multi-fastener semi-analytical or 2D finite element models that can later on be incorporated into reliability assessment or detailed finite element analysis of timber structures.

1.4. Outline of the paper

In order to develop the empirical-probabilistic model of steel-to-timber joints with screws, first, an experimental campaign was conducted varying the main parameters of influence, then the Richard-Abbott analytical models were used to fit the data and derive the regression parameters. Then, another bi-linear model was used to link the regression parameters to the load-to-screw axis angles. The experimental test set-up, the measurement technique, and the testing protocol are described in Section 2. The results of the experiments, i.e. the impact of the main parameters (the type of test set-up, the screw

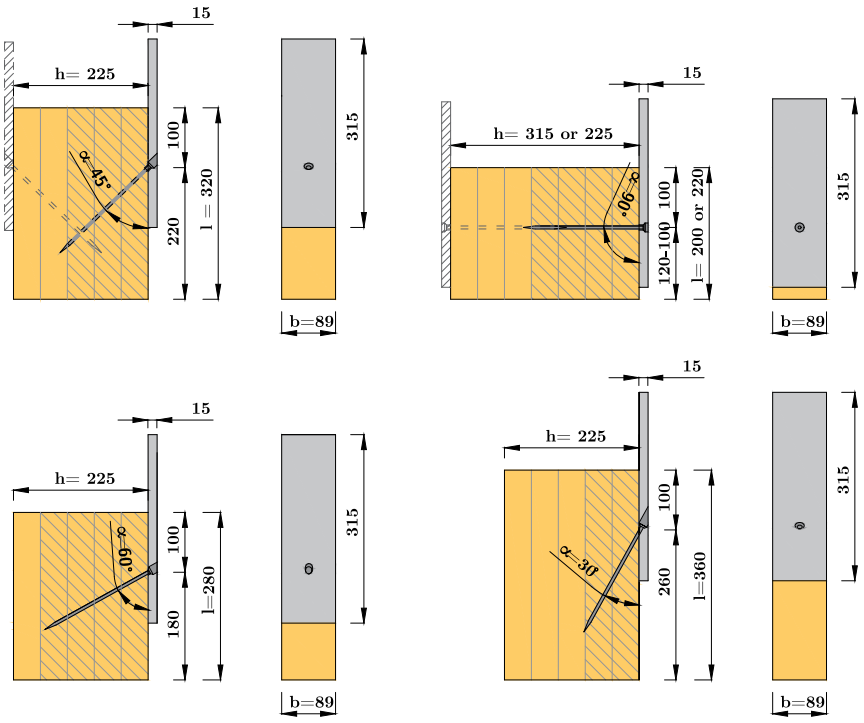

Fig. 1. Schematic plans and prospects of the specimen with single self-tapping screw. Highlighted lamellae indicate those used for the density calculations.

length, the friction in the shear plane, the torque, the load-to-screw axis angle, the moisture cycling conditioning, and the washer) on the non-linear load-deformation behaviour of joints with screws is discussed in Section 3. In Section 4, the developed empirical-probabilistic model on joints with screws is described and the mean values, coefficients of variation (CoVs) of the regression parameters and the correlation coefficient among them are reported.

Finally, Section 5 presents a comparison between the developed empirical-probabilistic model and the deterministic design parameters currently specified in EC5 [4]. The main conclusions and recommendations for future work are summarized in Section 6.

Table 1
Dimensions of the timber specimens.

Name of the timber specimen	b [mm]	h [mm]	l [mm]
B1	89	225	360
B2	89	225	320
B3	89	225	280
B4	89	225	220
B5	89	315	200
B6	89	180	250
B7	89	225	200
B8	89	315	450

2. Materials and methods

2.1. Materials

Steel-to-timber joints with screws were tested in twelve configurations in asymmetric and symmetric test set-up (Fig. 1). Glulam beams, made from GL30c class Norway Spruce, were designed to have a width of 90 mm. However, measurements showed that the actual width was 89 mm. While the width was always constant, the height and length of the specimens varied.

The beams followed the manufacturing standard EN14080 [31]. The glue was melamine glue (light glue joint). No systematic variation across the lamella positions was observed regarding the densities of the lamellae. All boards showed a nearly uniform density with a mean value that ranged from 455 to 480 $\frac{kg}{m^3}$.

The dimensions of the timber specimens are given in Table 1. The different lengths were selected to accommodate the screw with different load-to-screw axis angles. To capture both in-class and in-batch variability in the specimen density, the specimens were extracted from ten different beams, selecting multiple locations along each beam length.

The timber specimens were conditioned in a climate chamber for several weeks at a temperature (T) of 20 °C and at a relative humidity (RH) of 65%. The moisture content (MC) of the beams prior to testing was ≈11.6%, measured with a moisture sensor meter BES Bollman Combo 100.

To confirm the moisture meter readings, the oven-dry method was performed on conditioned specimens according to EN 13183-1 [32]. Three blocks (50 mm × 89 mm × 50 mm) were dried at (105 ± 3) °C until constant mass. The moisture contents determined by the oven-dry method agreed within (±2%) of the moisture meter readings. During the manufacturing of the timber specimens, small slices of 50 mm thickness were cut out of the beams after each specimen in order to determine the (wet) density distribution across the lamellas.

The steel plates used were made of S355 grade. The thickness was 15 mm, with a length of 315 mm and a width of 89 mm. In the general test series, the plain surface of the steel plates was used. In the test series with different values of friction coefficient, a steel plate with a rough surface was used to study the impact of the large value of the coefficient of friction, while a Teflon sheet as an interlayer was used to investigate the impact of a low value of friction coefficient. The two types of steel plates, one with a milled hole and the one with an elongated hole for the washer, are shown in Fig. 2(a).

The screws used in the tests are of type ASSYplus VG 4 FT from the company WÜRTH, the corresponding ETA-11/0190 is [33]. The selected lengths are 120 mm, 200 mm, and 400 mm. The geometrical and material characteristics of the screws reported in the ETA are given in Table 2. The geometrical characteristics (d, l) were verified on a random sample with a calliper (deviations <1%). The characteristic tensile

Table 2
Geometrical and mechanical characteristics of the screws according to ETA-11/0190 [33] and results from the experimental testing.

d [mm]	d_{core} [mm]	l [mm]	l_{eff} [mm]	$M_{y,k}$ [N m]	$M_{tor,k}$ [N m]	$f_{tens,k}$ [kN]	$f_{tens,m,exp}$ [kN]	$f_{tens,k,exp}$ [kN]
8	5.1 ±0.3	120/200/400	97/177/377	23	25	22	26.3	23

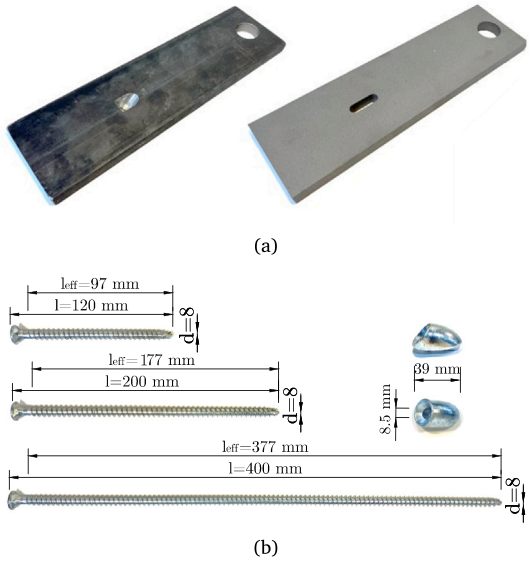

Fig. 2. (a) Steel plates with the milled hole and smooth surface (left), with the elongated hole for the washer and blast-profiled surface (right). (b): The 3 lengths of ASSYplus VG 4 FT screws and the washer.

resistance $f_{tens,k}$ was also benchmarked against experimental results from six 200 mm screws tested in accordance with ISO 6892 [34]. The characteristic value was then calculated following the statistical procedure of Eurocode 0, Annex D [35]. The mean value $f_{tens,m,exp}$ and the characteristic values $f_{tens,k,exp}$ so determined are also reported in Table 2.

The steel plates were milled accordingly in order to accommodate the seating of the screw heads for the load-to-screw axis angles 90°, 60°, 45°, and 30°. Washers according to ETA-11/0190 [33] were used for the series with a load-to-screw axis angle of 45°. These washers were inserted into elongated holes in the steel plates. The screws and washers are shown in Fig. 2(b).

In all the configurations, the screws were inserted without pre-drilling. The screws are positioned in the centre of the specimen width, which corresponds to an edge distance of $5 \cdot d$. The loaded edge distance $a_{3,t}$ is always equal to $12 \cdot d$. These values were within the limits prescribed by EC5 [4], both for axially and laterally loaded screws. This ensures that brittle failure is avoided even for larger displacements.

2.2. Test set-up

Two types of test set-ups were used in this study: symmetric and asymmetric. In both cases, the steel plate(s) were loaded in tension by the load cylinder while the timber specimen was clamped down by two rods of 16 mm diameter to the based plate (Fig. 3). The load was applied using a servo-hydraulic testing machine (MTS 327) with a capacity of 250 kN. The tests were performed taking the EN 12512 [36] as a reference, but performing the test always in a displacement-controlled mode with a speed of 1 mm/min. The loading history is composed of a first loading phase up to 40 % F_{est}, followed by an unloading phase down to 10% F_{est} and finally a re-loading phase up to the target displacement of failure (set to 15 mm) or to the displacement at which the head tear-off of the screw occurred. A first estimation of F_{est} was based on the formulae in [19], using the mean values of the properties in accordance with [37]. The estimated values were adjusted based on the first experiments for every load-to-screw axis angle. For the series with different load-to-screw axis angles and 10 to 20 repetitions, at the beginning of the test, a small value of tension force (≈0.15 kN) was applied to eliminate the initial slip of the curve due to the oversize of the hole. One or two load cells for the symmetric test set-up were incorporated within the testing machine to measure and record the loads.

In the asymmetric test setup, a single steel plate was screwed to one side of the timber specimen and loaded at a time. The load was recorded by an additional electric load cell incorporated within the testing machine, which had a capacity of 220 kN (Figs. 3(a) and 3(b)). In the symmetric test set-up, two steel plates were screwed to the opposing sides of the timber specimen and loaded simultaneously by an additional steel traverse (Fig. 3(c)). The steel traverse was hinged to prevent bending of the principal load cell in case of failure of one of the joints. Two load cells with a capacity of 50 kN were placed at the ends of the steel traverse and used to measure the loads on each steel plate.

2.3. Recording of the measurements

The deformations were measured in two ways: digital image correlation (DIC) was used in the test series with a few repetitions and various parameters, whereas linear variable displacement transducers (LVDTs) were applied in the test series with many repetitions. LVDTs were also used for specimens subjected to moisture cycling and the joints with rough steel plate surfaces.

The DIC with an ARAMIS-adjustable stereo camera system [38] was used to quantify the deformations on the entire surface of the front side of the specimens. The front side was painted in the area of interest with black speckles on a white background to achieve a high contrast. Images were taken with a frequency of 1/2 Hz. Each image was assigned to a specific force value via an analog output signal of the testing machine, which allowed to obtain a load–displacement curve for each test. In this way, the movement of all the parts of the test set-up (timber specimen, screw head, front and side surface of the steel plate) could be tracked in all three dimensions. The analysis confirmed the absence of any out-of-plane specimen movement and simultaneously, it provided the data for complete load–displacement curves by tracking two reference points: one on the steel plate and one on the timber member.

In the test series with more repetitions, the relative displacement between the steel plate and the timber (parallel to the shear plane) was measured using LVDTs places on each side of the joint. Two additional LVDTs were placed at the top and bottom of the steel plate to monitor the movements of the steel plate perpendicular to the shear plane. The displacement was measured relative to the steel plate and in correspondence with the position of the screws (approximately $12 \cdot d$ from the top border of the timber specimen) with a frequency of 8 Hz.

2.4. Test series and parameters

The influence of the following parameters of influence on the load-deformation curves of the joints has been studied in the different test series: the test set-up, the screw length, the friction, the torque, the load-to-screw axis angle, the moisture cycling and the washer. A small number of repetitions (3) was considered sufficient in these series, enough to obtain a representative average and see whether a factor influenced the load–displacement curve.

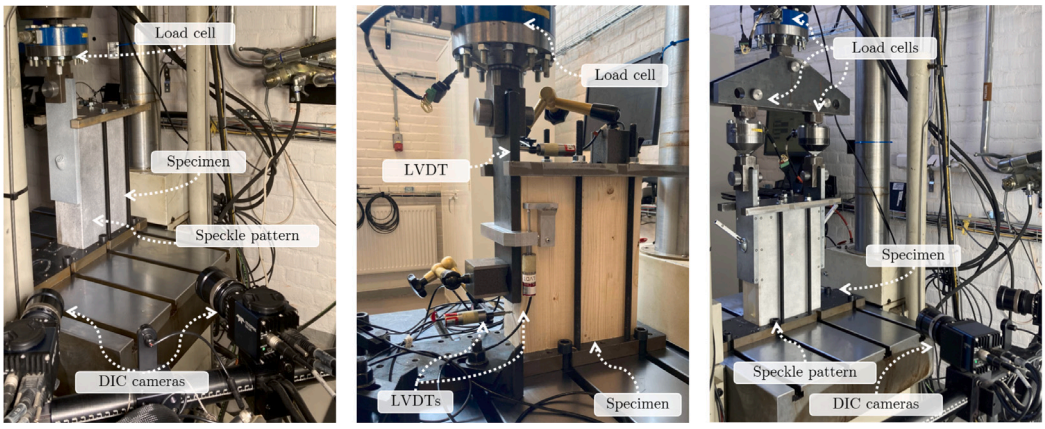

Fig. 3. The three test set-up used in the study. (a): Asymmetric test set-up and DIC system; (b): Asymmetric test set-up and LVDTs; (c): Symmetric test set-up and DIC system.

By contrast, to decide the number of repeated tests to determine the variability for different load-to-screw axis angle of the baseline configuration (200 mm screws, medium torque, smooth steel plate), a Monte Carlo study was conducted. A lognormal distribution with CoV = 30% was assumed, and 5000 runs per candidate sample were performed. The output was that 20 tests are required for the EN 14358 [39] characteristic value (5%-fractile) to lie within ±25% of its true value at the 5% significance level. With only 10 tests, the confidence interval increases to ≈35 %. Therefore, 20 tests were judged enough to satisfy the confidence interval requirements according to EN 14358, while 10 tests still provide useful exploratory insight.

The label assigned to each specimen is explained in Fig. 5. An overview of the varied parameters with the corresponding number of repetitions is given in Table 3.

To determine which side of the timber specimen would be used for the joint, the wet densities of the screw-bearing lamellae were compared. Each lamella was weighed after conditioning it at T = 20 °C and RH = 65%, and its external dimensions were measured and the density was calculated. For example, in the five-lamella lay-up, only the three lamellas where the screws was embedded were relevant. Their mean density was calculated separately for the left (sx) and right (dx) sides of the specimen. The lamellae used in the density calculation for each load-to-screw axis angle are now also highlighted (grey pattern) in Fig. 1. Whenever possible, the side was selected in such a way that the average lamella density for each series remained comparable to the others, thereby isolating the effect of the studied parameter. The average value of density for each joint and series is illustrated in Fig. 4.

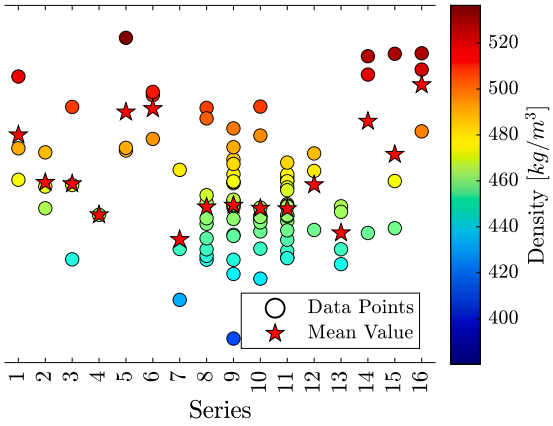

Fig. 4. Density distribution of each series.

3. Results and discussion

The following presents the results of the experiments, and in particular, the influence of the investigated parameters of influence on the load–displacement behaviour of the joints. In the initial DIC series, applying a small compressive force resulted in an early slip due to the hole clearance and the washer clearance. Fig. 7 shows one repetition with a solid line and the other two with dashed lines. For joints that exhibited initial slip due to clearance, the load–displacement curves were realigned at 10% of the estimated load-carrying capacity, which enhanced both visualization and interpretation of the data. Additionally, the unloading-reloading phase has been omitted from the graph for the same purpose.

3.1. Symmetric versus asymmetric test set-up

As a first parameter to evaluate, the symmetric and asymmetric test set-ups were compared. The load–displacement curves of symmetric and asymmetric are shown in Fig. 6 for the load-to-screw axis angle of 45° and 90°.

For the asymmetric test set-up, the single curve follows the load–displacement of the joint and captures the respective failure mode of the screw, such as head tear-off (HTO) failure or withdrawal failure (WITH). Two load–displacement curves for the symmetric test setup can be determined, one for each joint. Depending on the failure modes of the screws, only one of the two curves will capture the failure (and the load-carrying capacity) of the respective joint, whereas the other will turn into an unloading phase without reaching the load-carrying capacity of the joint. In Table 4, key performance parameters were calculated for symmetric and asymmetric tests, and values were compared; these are the elastic slip-modulus K_{10-40}, the load-carrying capacity F_{max}, and the ultimate displacement (v_u). K_{10-40} was as the secant slip-modulus between two load levels (10% and 40% of the load-carrying capacity F_{max}). v_u is the maximum displacement recorded before abrupt failure (or in the case of the failure due to the withdrawal of the screws, the displacement in correspondence of the 30% drop after reaching the load carrying-capacity) [36,40].

The relative difference, Δ, between the asymmetric (ASY) and symmetric (SYM) setup is defined as:

$$\Delta = \frac{X_{\mathrm{ASY}} - X_{\mathrm{SYM}}}{X_{\mathrm{ASY}}} \quad (1)$$

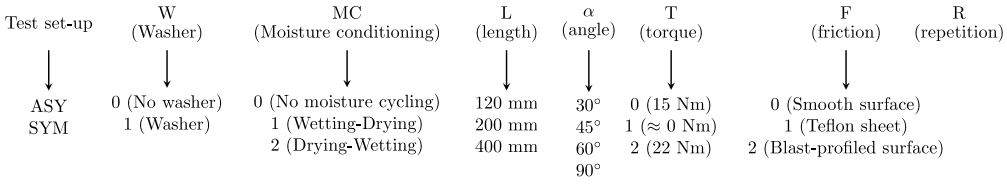

Fig. 5. Description of the label.

Table 3
Summary of the specimens tested. In red, the parameters varied in each series.

Specimen	Series	Test Set-up	W	MC	L [mm]	α [°]	T	F	R
B2	1	SYM	1	0	200	45	0	0	3
B5	2					90			
		Test Set-up	W	MC	L [mm]	α [°]	T	F	R
B5	3	ASY	0	0	200	90	2	0	2[a]
	4			1					3
B2	5			2					
		Test Set-up	W	MC	L [mm]	α [°]	T	F	R
B6	6	ASY	1	0	120	45	0	0	3
B2	7				200				
B8	8				400				
		Test Set-up	W	MC	L [mm]	α [°]	T	F	R
B1	9	ASY	0	0	200	30	0	0	10
B2	10					45			20
B3	11					60			10
B5	12					90			20
		Test Set-up	W	MC	L [mm]	α [°]	T	F	R
B5	13	ASY	0	0	200	90	1	0	3
	14						2		
		Test Set-up	W	MC	L [mm]	α [°]	T	F	R
B5	15	ASY	0	0	200	45	0	1	3
B7	16							2	

[a] One repetition out of three was omitted because the applied torque was uncertain.

Table 4
Key parameters for symmetric (SYM) and asymmetric (ASY) test set-up for the two load-to-screw axis angles. Δ is the relative difference (Eq. (1)).

Parameter	Angle [°]	SYM (mean ± SD)	ASY (mean ± SD)	Δ [%]
K_{10-40} [kN/mm]	45	9.2 ± 1.7	9.5 ± 2.0	4
	90	1.55 ± 0.3	2 ± 0.7	23
F_{max} [kN]	45	22.6 ± 0.5	21.4 ± 1.3	6
	90	12.4 ± 0.6	11.4 ± 0.7	9
v_u [mm]	45	3 ± 0	3 ± 0.3	0
	90	12.8 ± 0.5	10.21 ± 1.4	26

where X_{ASY} is the mean value of the selected key parameter for the asymmetric test set up (ASY) and X_{SYM} is the mean value of the selected key parameter for the asymmetric test set up (SYM). The asymmetric test setup produced load–displacement curves comparable to the symmetric reference in terms of key parameters. Relative differences were 6% and 25% for the initial slip-modulus K_{10-40}, 6% and 9% for the load-carrying capacity F_{max}, and 7% and 26% for the ultimate displacement v_u. The summary of the evaluation is reported in Table 4. The differences were judged to be within the variability associated with the mechanical properties of timber. Hence, the asymmetric test setup was considered suitable for determining the impact of the different parameters on joint behaviour.

3.2. Screw length

The effect of screw length on the load–displacement behaviour of joints with a load-to-screw axis angle of 45° is depicted in Fig. 7(a). The elastic slip-modulus was not sensitive to the screw length, and the main differences regarded the load-carrying capacity and the failure of the joints. For screws with a length of 120 mm, the load–displacement curve exhibited an initial linear region followed by a pronounced softening behaviour. The failure occurred only due to the withdrawal of the screw. In contrast, screws with a length of 200 mm displayed a similar load–displacement curve but demonstrate a higher load-carrying capacity and brittle behaviour due to the occurrence of the head tear-off failure. The load-carrying capacity increased as the screw length was raised from 120 mm to 200 mm. Beyond that, it remained constant because failure then occurred due to head tear-off, indicating that the screw tensile capacity was reached.

3.3. Friction

In order to study the effect of friction on the shape of the load–displacement curve, three variations of friction in the contact surface were tested (Fig. 7(b)). A low value of friction was obtained by placing a Teflon sheet as an interlayer between the steel plate and the timber specimen, an average value of friction coefficient was obtained with the smooth (untreated) steel plate surface, and the timber specimen, and a high value of friction coefficient was obtained producing a blast-profiled steel plate surface. The requested steel plate treatment is classified as Sa 2½(Very Thorough Blast Cleaning) according to ISO 8503 [41].

The joints with Teflon sheet presented slightly less stiff behaviour in the elastic stage and comparable load-carrying capacity as in the case of the average friction coefficient. The series with the blast-profiled steel surface showed stiffer behaviour and considerably higher load-carrying capacities than those with the Teflon sheet and the smooth surface steel

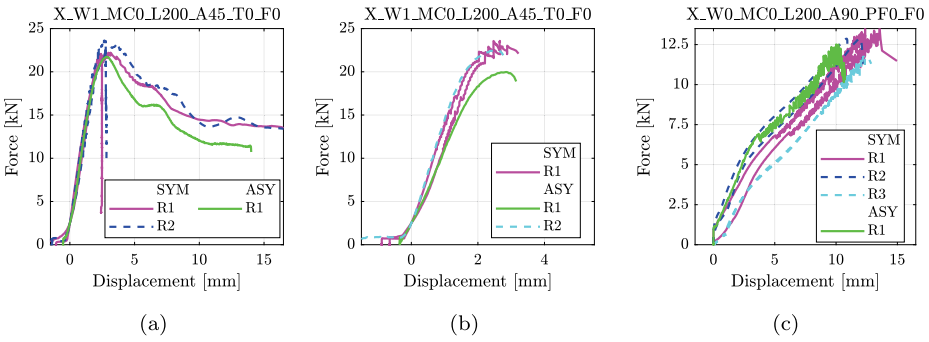

Fig. 6. (load–displacement joint)-displacement curves from the symmetric versus asymmetric test set-up. (a) load-to-screw axis angle 45° (withdrawal failure), (b) load-to-screw axis angle 45° (head tear off failure), (c) load-to-screw axis angle 90° (head tear off failure).

plate. In both series the failure was due to both withdrawal failure and head-tear-off of the screws.

With Eq. (2) from [15] the shear capacity of joint F_v with a screw can be calculated. α is the load-to-screw axis angle, F_{ax} is the axially capacity of the screws, determined as the minimum between the withdrawal capacity and the tensile capacity of the screw, μ is the steel-to-timber friction coefficient, F_{lat} is the lateral capacity of the screw. Using the Eq. (2) from [15] and assuming that zero friction ($\mu = 0$) applies to the series with the Teflon sheet, led to the average value of friction coefficients of 0.16 and 0.54 for the cases with natural smooth surface and with rough surface of the steel plates, respectively.

$$F_v = F_{lat} \cdot (\cos\alpha - \mu \cdot \sin\alpha) + F_{ax} \cdot (\sin\alpha + \mu \cdot \cos\alpha) \quad (2)$$

3.4. Torque

Three torque levels of, 60% (15 N m), and 90% (22 N m) of $M_{tor,k}$ were tested, and the effects on the load–displacement curves are shown in Fig. 7(c). A torque wrench was used to ensure the appropriate pre-tensioning moment. Generally, in steel-to-timber joints, a tight joint fit is intended. Increasing the torque during insertion of the screws means increasing the pre-stressing force to which the screw is subjected. The torque and pre-stressing should be sufficient to prevent slip in the joint. However, the torque should not exceed 2/3 of the torsional resistance of the screw, according to ETA-11/0190 [33].

When the force perpendicular to the sliding plane increased for higher torque levels, the joint behaved stiffer at the beginning of the load–displacement curve, resulting in a rigid region without joint deformation. This rigid region was more pronounced when torque was applied to tighten the steel plate to the timber, being more evident in the case with a torque equal to 22 N m. Not all the joints with 15 N m of torque showed the rigid region, indicating that this phenomenon is affected by variability.

Moreover, the joints without torque and approximately zero clamping force showed no initial rigid region and a more flat post-yielding behaviour, followed by a hardening behaviour. The latter corresponds to the rope effect, present in the case of other torque values, which appears at a larger displacement compared to the other joints with larger torque. As observed by splitting the specimen, in the case of zero torque, the bending of the screws was more pronounced than in the other cases. In contrast, for the other joints subjected to the torque of 15 N m and 22 N m, the screw remained straighter compared to the screw without prestressing, due to the prestressing force.

3.5. Load-to-screw axis angle

The effect of the load-to-screw axis angle on the load–displacement behaviour is illustrated in Fig. 7(d). Joints with load-to-screw axis angle of 90° showed less stiff behaviour at the beginning of the load–displacement curve but more ductile behaviour, being the curve characterized by a pronounced hardening trait in the plastic region. Failure consisted in the development of two plastic hinges before the head tear-off failure of the screw. For a load-to-screw axis angle of 60°, the load–displacement curves exhibited a stiffer initial response, higher load-carrying capacity, and considerably reduced ductility. In contrast, joints with a 45° load-to-screw axis angle showed a similar overall curve shape but with an even stiffer initial response and further reduced ductility. In the tests with this angle, failure occurred either by head tear-off or withdrawal of the screw. When withdrawal was the failure mode, the curve displayed a marked softening after reaching the load-carrying capacity. For joints with a 30° load-to-screw axis angle, the curve was similar to that of the 45° case, though it was marginally stiffer and exhibited slightly lesser ductility. In Table 5, the failure modes occurring for each test configuration are reported. The withdrawal failure occurred in the 40% of the tests for a load-to-screw axis angle of 30°, while it occurred only one time for a load-to-screw axis angle of 45°. For the load-to-screw axis angle of 60° and 90°, the failure only occurred by head tear-off failure.

Table 5
Total number of the tests for each load-to-screw axis angle and the number of tests that failed due to the withdrawal of the screw (WITH) and due to the head-tear off of the screw (HTO).

α [°]	No. test	WITH	HTO
30	10	4	6
45	20	2	18
60	10	0	10
90	20	0	20

3.6. Moisture cycling

A combination of the effect of friction and the torque level causes the initial rigid region in the load–displacement curves of joints with screws inclined at 90°. Six specimens, each loaded with 22 N m of torque, underwent moisture cycling to investigate the effects of moisture-induced swelling and shrinkage on the initial rigid region of the load–displacement curve. The climate extremes (temperature T° and relative humidity RH %) were selected to reflect the limits of service class 2 moisture conditions.

All specimens were first conditioned at 20 °C and 65% RH until moisture-content changes fell below 0.10% over two consecutive days (initial MC ≈12%).

The six specimens (each torqued to 22 N m) were then split into two groups of three:

First serie (Wetting → Drying):

- *Wetting cycle:* 20 °C, 95% RH until equilibrium (≈18% MC).
- *Drying cycle:* 20 °C, 40% RH until equilibrium (≈8% MC).

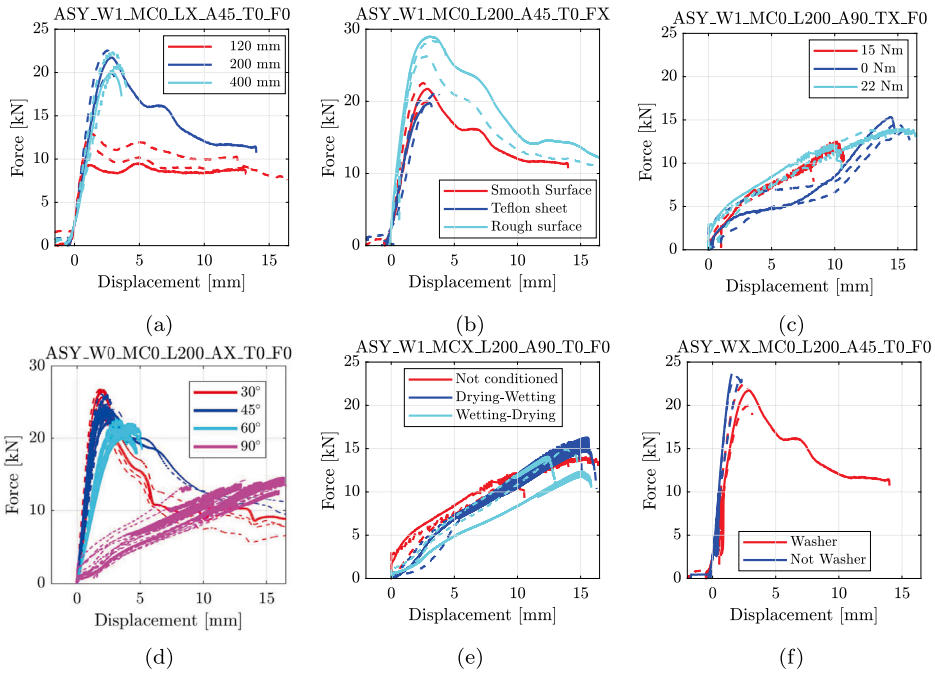

Fig. 7. Effect of the different parameters of influence on the load–displacement curve. (a) the effect of the screw length, (b) the effect of the friction, (c) the effect of the torque, (d) the effect of the load-to-screw axis angle, (e) the effect of the moisture cycling, (f) the effect of the washer.

- *Re-conditioning:* 20 °C, 65% RH until return to initial MC (≈12% MC).

Second series (Drying → Wetting):

- *Drying cycle:* 20 °C, 40% RH until equilibrium (≈8% MC).
- *Wetting cycle:* 20 °C, 95% RH until equilibrium (≈18% MC).
- *Re-conditioning:* 20 °C, 65% RH until return to initial MC (≈12% MC).

Each conditioning phase lasted roughly three months; specimen masses were recorded before conditioning and every two days thereafter. A phase was deemed complete when the mass change over 48 h was less than 0.10%. The equilibrium MC was quantified by reference blocks (dimensions 45 × 89 × 50 mm) of known oven-dry mass.

The results are illustrated in Fig. 7(e). In the first series, the steel plates were loose at the end of the cycle, while in the second series, the clamping of the screws still exercised some grip on the steel plate. This suggested that performing the wetting cycle before the drying one resulted in more residual deformations due to swelling/drying than the opposite case. In the case of the joints subjected to the wetting-drying cycle, the initial region disappeared or decreased if compared to the non-conditioned specimen. The second set of joints, in terms of load–displacement curves, led on average to slightly lower ductility and load-carrying capacity. A small initial region was still present in one of the load–displacement curves.

3.7. Washer

The joints with and without a washer were compared in the case of a load-to-screw axis angle of 45° (Fig. 7(f)). The two types of joints did not differ regarding elastic slip-modulus, load-carrying capacity, ductility, and failure mode. The difference regards the initial region of the load–displacement curve at a low load level (before reaching 10% of the load-carrying capacity). In fact, in the case of the washer, the hole in the steel is larger than in the case of the milled hole. Consequently, the displacement had to increase more before the parts of the joints would get in contact with each other.

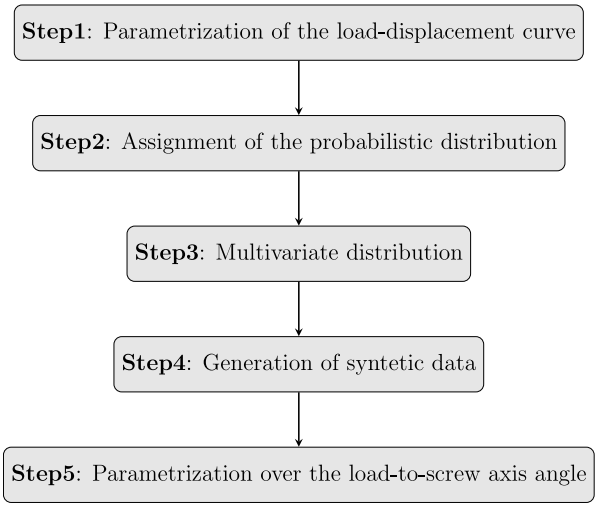

Fig. 8. Flowchart. Derivation of the empirical-probabilistic model in the 5 steps.

4. Analysis

An empirical-probabilistic model was established, which allows for accurate and reliable characterization of steel-to-timber joints with screws. By modelling the load–displacement curve, other characteristics of the curve can be modelled, such as initial slip, initial stiffening, or post-peak softening behaviour. Only the tests with many repetitions and different load-to-screw axis angle, where the LVDTs were employed as a measurement technique, were used to construct the model. Some of the results presented in this paper were partially reported in a previous scientific paper, specifically the determination of the empirical-probabilistic modelling and the description of the test data with different load-to-screw axis angles [42].

The parametrization of the load–displacement curves follows a five-step approach, similar to what has been described in [25]. In Step1, a parametrized analytical expression f is used to fit each

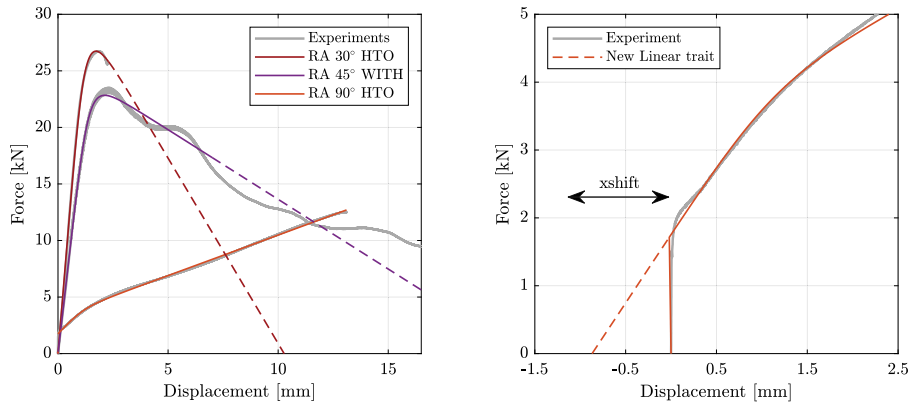

Fig. 9. (a) typical load–displacement curves for different load-to-grain angles, (b) approximation of the initial rigid region by a linear trait.

load–displacement data.

$$y_\alpha = f(m_{1,\alpha}, m_{2,\alpha}, m_{3,\alpha}, \dots, m_{i,\alpha}) \tag{3}$$

The m parameters of the model are in function of the parameter of influence (in this case, the load-to-screw axis angle). Then in Step2 a probabilistic distribution is assigned to each of the parameters, based on empirical fit and theoretical consideration.

$$m_i \sim \text{Dist(parameters)} \tag{4}$$

In Step3, the dependencies among the m parameters are taken into account. If the correlation between variables is considered, the parameters should be sampled together from a joint probability distribution of the correlated parameters. In order to obtain the correlated values, the correlation matrix can be factorized using the Cholesky decomposition:

$$\mathbf{C} = \mathbf{L}\mathbf{L}^T \tag{5}$$

where $\mathbf{C}$ is the correlation matrix, and $\mathbf{L}$ is the Cholesky matrix (upper or lower triangular). Then the correlated random variables are given by:

$$\mathbf{L}\mathbf{X} = \mathbf{Y} \tag{6}$$

In Step4, synthetic data are generated, providing $1, 2, \dots, g$ new load–displacement curves. The number of the sampled curves g is chosen in a way to be statistically representative of the variation of the dataset.

$$\begin{aligned} y_1 &= f(m_{11,\alpha}, m_{21,\alpha}, m_{31,\alpha}, \dots, m_{i1,\alpha}) \\ y_2 &= f(m_{12,\alpha}, m_{22,\alpha}, m_{32,\alpha}, \dots, m_{i2,\alpha}) \\ y_g &= f(m_{1\ g,\alpha}, m_{2\ g,\alpha}, m_{3\ g,\alpha}, \dots, m_{ig,\alpha}) \end{aligned} \tag{7}$$

In Step5, a new analytical model was applied to each of these m coefficients to give a regression between the coefficients and the load-to-screw axis (α).

$$m_i = f(b_1, b_2, \dots, b_n) \tag{8}$$

This allows the interpolation of the values of the parameters and their variability also in correspondence with different load-to-screw axis angles. In the end, the load–displacement curves, in function of the load-to-screw axis angle and the related variability, can be expressed by a matrix of $m \cdot n$ coefficients. The summary of all the steps are illustrated in the flowchart in Fig. 8.

4.1. Parametrization of the load–displacement curve (Step1)

To fit the load–displacement curves of the joints the Richard Abbott model is selected since it is able to also represent the intrinsic variability of the data.

The Richard-Abbott model is a function of four parameters (Eq. (9)): K_{in} represents the initial inclination of the curve, K_p is the inclination in the plastic region, i.e. after the peak (or yield point) of the curve, and the shape parameter a_1 controls the shape of the transition between the elastic and the plastic region.

$$F(v) = \frac{(K_{in} - K_p) \cdot v}{(1 + (\frac{(K_{in}-K_p)}{F_t} \cdot v)^{a_1})^{\frac{1}{a_1}}} + K_p \cdot v \tag{9}$$

For every test curve, the parameters K_{in}, F_t, K_p and a_1 were obtained by non-linear least-squares fitting of Eq. (9) to the measured load–slip data, as follows:

$$\min_{K_{in}, F_t, K_p, a_1} \sum_{i=1}^{n} \left[F_{\text{exp},i} - F_{\text{model}}(v_i; K_{in}, F_t, K_p, a_1)\right]^2 \tag{10}$$

where $\{F_{exp,i}\}_{i=1}^{n}$ and F_{model} are the vector of force measurements and of the analytical force, respectively. The optimization was carried out with the `fmincon` algorithm of MATLAB using the default convergence criteria.

The range of the load–displacement curve for the regression was chosen up to a 30% load drop from the load-carrying capacity for the curve corresponding to joints with screws arranged at an angle and characterized by a withdrawal failure. However, the fit of the curve appeared to be satisfactory even after the endpoint of the displacement regression range (Fig. 9(a)).

The entire load–displacement curve up to load-carrying capacity has been used for the tests with screws perpendicular to the grain and up to the load drop for tests with inclined screws but characterized by head-tear-off failure. For curves with shorter softening branches, the parameter K_p, defined as the asymptote of the derivative of the Richard-Abbott equation for very large displacement values, is difficult to characterize and does not possess a physical interpretation. Nonetheless, K_p can still be computed via non-linear regression (as shown by the dashed line in Fig. 9(a)). Moreover, an additional regression parameter must be introduced: the displacement at failure v_u, at which point the regression curve is truncated. For the load–displacement curve of joints with screws inclined at 90°, ad additional parameter x_{shift} was used to shift the curve horizontally and represent the initial rigid region (Fig. 9(b)).

4.2. Assignment of probabilistic distribution (Step2)

In Step2, a probability distribution was assigned to each regression parameter. This is necessary for the model to accurately predict the behaviour of the joints and the related variability. The distribution was chosen based on different criteria: empirical fit, theoretical consideration, and practical considerations.

Table 6
Overview of the parameters and their CoV for different load-to-screw angles.

α [°]	Failure	K_{in} [kN/mm]	F_t [kN]	K_p [kN/mm]	a_1 [–]	v_u [mm]
30	HTO	18.35 (0.21)	35.1 (0.06)[a]	−4.10 (0.14)[a]	8.10 (0.53)[a]	2.53 (0.07)
	WITH		32.87 (0.05)	−4.15 (0.12)	10.25 (0.15)	3.90 (0.08)
45	HTO	16.24 (0.14)	38.25 (0.24)	−4.90 (0.56)	5 (0.31)[b]	2.97 (0.13)
	WITH		26.32[c]	−1.31[c]	6.33[c]	6.35[c]
60	HTO	8.84 (0.10)	39.80 (0.25)	−3.64 (0.37)	4.19 (0.29)	4.47 (0.10)
90	HTO	1.63 (0.32)	2.75 (0.75)	0.76 (0.20)	7.26 (0.58)	13.85 (0.16)

The values of v_u for the withdrawal failure of the screws (WITH) refer to the regression interval used to fit the Richard-Abbott model.
x_{shift} has a significant value only for steel-to-timber joints with screws arranged at 90°: −0.19 (0.68). It can be approximated to zero for all the other cases.

[a] One outlier.

[b] Three outliers.

[c] Only the mean value is provided since only two tests failed due to the withdrawal of the screw.

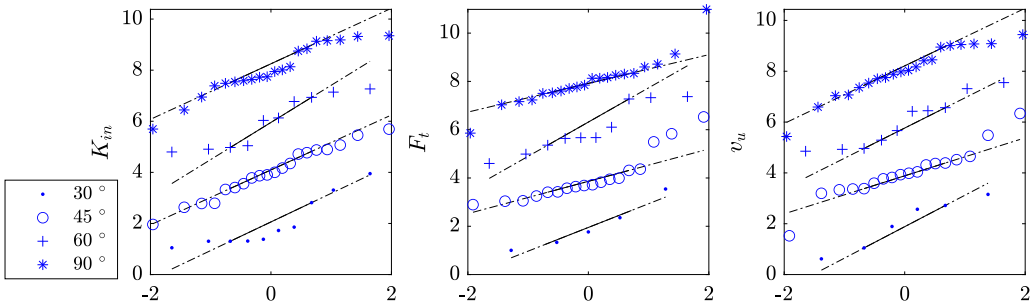

Fig. 10. Q-Q Plots for some parameters of the model for each of the load-to-screw axis angle.

Table 7
Correlation matrix of the regression parameter in function of the load-to-screw axis angle.

α	30°				45°				60°				90°				
	F_t	K_p	a_1	v_u	F_t	K_p	a_1	v_u	F_t	K_p	a_1	v_u	F_t	K_p	a_1	v_u	x_{shift}
K_{in}	0.72	−0.72	−0.85	−0.77	0.42	−0.49	−0.43	−0.71	−0.25	0.26	0.14	−0.79	0.10	0.28	−0.19	−0.50	0.18
F_t	1	−1.00	−0.60	−0.47	1	−0.99	−0.81	−0.15	1	−0.95	−0.93	0.60	1	−0.75	−0.40	0.10	−0.12
K_p		1	0.60	0.47		1	0.8	0.19		1	0.86	−0.48		1	0.40	−0.34	0.08
a_1			1	0.46			1	−0.07			1	−0.51			1	0.02	0.13
v_u				1				1				1				1	0.55
x_{shift}																	1

A lognormal distribution looked suitable to represent the variability associated with K_{in}, F_t, a_1, and v_u. The values of these parameters are always expected to be positive; thus, a lognormal distribution was selected. A normal distribution is assigned to the parameter K_p since it can assume both positive and negative values. In fact, when the screws are loaded both laterally and axially, K_p reflects the softening behaviour (indicated by a negative mean value), whereas when the screws are only laterally loaded, it reflects hardening behaviour (indicated by a positive mean value). The log-normalized and the normalized data for the parameter K_{in}, K_p, and v_u for all the values of load-to-screw axis angles are plotted in Fig. 10 respectively. An offset was applied to each dataset to visualize multiple Q-Q plots within a single figure without overlapping. The distribution characteristics (the mean value and CoV) for each value of load-to-screw axis angle are summarized in Table 6.

4.3. Calculation of the correlation matrix (Step3)

Given the variability of the parameters, it is necessary to consider the correlations among them to generate the corresponding load–displacement curves. This can be done using the Pearson coefficient, and the (shortened) correlation matrices are given for selected cases in Table 7. From the determined regression parameters and the correlation among them, load–displacement curves using the Richard-Abbott model can be generated.

4.4. Generation of synthetic load–displacement data (Step4)

Once the probabilistic distributions are assigned for every parameter of the Richard-Abbott model, a synthetic curve can be randomly generated from the multivariate distribution. Due to the correlation among the parameters, the load–displacement curve corresponding to the i-fractile of the curve envelope does not match the curve generated by using the i-fractile values of each parameter. For example, Fig. 11 shows the envelope defined by the 5th-fractile, 95th-fractile load–displacement curves, together with the mean curve.

4.5. Parametrization over the load-to-screw axis angle (Step5)

The relation between the parameters and the load-to-screw axis angle was modelled in Step5, comparing one analytical model (Hankinson model), a bi-linear function and a design formula. The Hankinson model [43] was originally developed to link the wood grain orientation to the compressive strength of wood Eq. (11). P_0 and P_{90} are the parameters at the principal material directions, i.e., at the boundaries of the regression curve. Most of the previous investigations focused on the modification of the Hankinson approach or bi-linear relationships [26,30] for modelling the behaviour of parameters over the load-to-grain angle for axially loaded screws and the embedment behaviour of dowels.

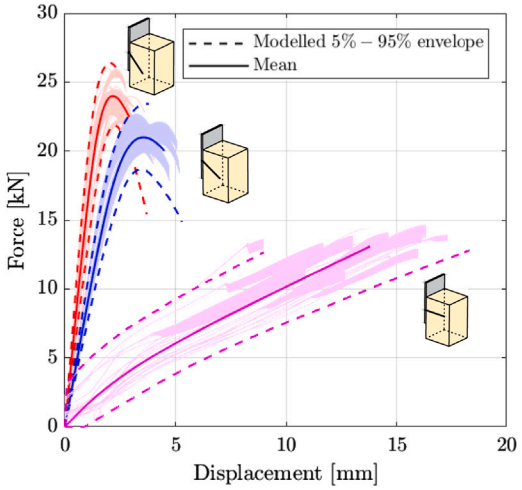

Fig. 11. Generated load–displacement for load-to-screw axis angles of 90°, 60°, and 45°.

Table 8
Parameters of the bi-linear model.

	K_{in} [a] [kN]	F_t [kN]	K_p [kN/mm]	v_u [mm]	a_1 [–]
$P_{mean,1,\alpha}$	14.37	38.00	−4.32	3.33	5.79
$P_{mean,2,\alpha}$	−24.36	−67.19	9.69	20.12	3.33

[a] The mean values of the parameter K_{in} were better approximated by Eq. (13). The fitted values are: $K_{SLS,ax} = 23.29$ [kN/mm] and $K_{SLS,v} = 2.19$ [kN/mm].

The Hankinson model does not exhibit a plateau. Consequently, to capture the nearly constant behaviour of parameters—such as F_t, K_p and v_u—between 30° and 60°, the Hankinson model was compared with a bilinear function with an anchor point at 60°. This bilinear approach is characterized only by two regression parameters and effectively represents the sharp drop that often occurs between 60° and 90°.

$$P_{\alpha,\text{mean}} = \frac{P_{0,\text{mean}} \cdot P_{90,\text{mean}}}{P_{0,\text{mean}} \cdot (\sin\alpha)^2 + P_{90,\text{mean}} \cdot (\cos\alpha)^2} \tag{11}$$

$$P_{\alpha,\text{mean}} = \begin{cases} P_{mean,1,\alpha} & \text{if } 0° \le \alpha \le 60°, \\ P_{mean,2,\alpha} \cdot \alpha & \text{if } \alpha > 60°. \end{cases} \tag{12}$$

For the parameter K_{in}, the design formula (Eq. (13)) for the slip-modulus for inclined-arranged screws is also compared (see Table 8).

$$K_{SLS} = K_{SLS,ax} \cdot \sin\alpha \cdot (\sin\alpha + \mu \cdot \cos\alpha) + K_{SLS,v} \cdot \cos\alpha \cdot (\cos - \mu \cdot \sin\alpha) \tag{13}$$

where $K_{SLS,ax}$ and $K_{SLS,v}$ are the slip-modulus of axially loaded and laterally loaded screws according to the new generation of EC5 [44].

The models were compared for all the regression parameters in Fig. 12. The Hankinson formula overfitted the data for the mean values of the parameter K_{in}, F_t and K_p, as can be noted by the wavy shape between the values of 30° and 60°. The bi-linear model captured the pseudo-plateau of the median between 30° and 60°, followed by a descending trait for all the mean values of the parameters F_t, K_p and v_u. The analytical formula best captured the trend, following the data most accurately for the mean values of K_{in}.

5. Discussion

5.1. Comparison with standards

The following chapter compares the results derived from the empirical-probabilistic model to the current generation of EC5. Employing an empirical probabilistic model rather than using raw experimental data means capturing a full distribution behaviour of the data.

Table 9
Values of μ for different values of ψ at different load levels.

	$0.7 \cdot F_{max}$	$0.8 \cdot F_{max}$	$0.9 \cdot F_{max}$	$1 \cdot F_{max}$
$\psi = 1$	1.05	1.2	1.35	1.5
$\psi = 2$	1.10	1.44	1.82	2.25
$\psi = 3$	1.15	1.73	2.46	3.38

Therefore, the 1000 synthetic curves are compared with the definition for slip-modulus at ULS and the relative and absolute definition of ductility. The calculation of the load-carrying capacity was excluded since this aspect is widely investigated in the literature [15,21].

5.2. Slip-modulus

At ULS, the slip-modulus is reduced to two-thirds of K_{SLS}, so that $K_{ULS} = \frac{2}{3} \cdot K_{SLS}$. Both K_{SLS} and K_{ULS} are empirically derived, in particular, the formula of K_{ULS} is based on the observations of [45] on nailed joints. In [45] the slip modulus at 0.5 mm and 1.0 mm joint deformation are compared based on load-deformation curves on nailed joints derived in [46]. For comparison with this definition, the ratio between the two secant stiffness ($K_{0-1\text{ mm}}/K_{0-0.5\text{ mm}}$) as specified by [45]. The related variability were calculated and are shown in Fig. 13(a).

The initial rigid region that characterizes the joints with screws at 90° was excluded from the analysis. In addition to the values of the boxplot, the 5 %– and 95 %–-fractiles are given and marked with a cross. The variability of the ratio $K_{0-1\text{ mm}}/K_{0-0.5\text{ mm}}$ decreases with increasing load-to-screw axis angles. The mean value ranges from 0.9 to 1, showing that the classic definition of K_{ULS} is not suited for these types of joints. This happens since both $K_{0-1\text{ mm}}$ and $K_{0-0.5\text{ mm}}$ are secant at load levels in the elastic range of the load–displacement curve. A comparison is made with the ratio K_{0-max}/K_{10-40}. K_{10-40} is the stiffness in the elastic range; for this reason, in the case of the joints with screws at 90°, the stiffness is a secant through 10 %– and 40 %– of the yielding point. The mean of the ratio is, in this case, close to the prescribed ratio of 2/3 between the load-to-screw axis angle of 30° and 60°. However, in particular for the load-to-screw axis angle of 90°, the variance of the ratio is much larger. The ratio $K_{0-max}/K_{mean,10-40}$ presents similar results to K_{0-max}/K_{10-40} but a lower variance for the case of the load-to-screw axis angle of 90°.

K_{ULS} linearizes the load–displacement curves of joints, considering the diminishing value of the slip-modulus for increasing load level. However, this factor does not consider the different joint typologies and the utilization ratio of each joint. In Eurocode 3 (EC3) [47], the rotational stiffness of steel joints is defined in the function of utilization ratio. The slip-modulus at ULS is defined as $\frac{K_{SLS}}{\mu}$ there μ is defined as the following:

$$\mu = \begin{cases} 1 & \text{if } F_{Ed} \le 2/3 \cdot F_{Rd} \\ \frac{1.5 F_{Ed}}{F_{Rd}}^{\psi} & \text{if } F_{Ed} \ge 2/3 \cdot F_{Rd} \end{cases} \tag{14}$$

μ is a factor that describes the decay of the slip-modulus K_{10-40} with increasing load level. In EC3 the factor is written in function of the acting moment on the joint and the bending resistance of the joint. Herein, it is written in function of the acting The load–displacement curves were realigned F_{Ed} and the design value of the load-carrying capacity of the joint F_{Rd}. In EC3 ψ is defined for each type of steel joints (welded, bolted). The bigger the factor is, the less rapidly the stiffness decreases with increasing load level. Some example of the μ factor are reported in Table 9. For the case $\psi = 1$, and when the load reaches the load-carrying capacity of the joint, the approach of EC3 corresponds to the reduction of 2/3 currently proposed by EC5.

In Fig. 13(b), the evolution of the stiffness ratio with increasing load levels is illustrated. For joints with screws positioned at 90°, the evolution of the secant stiffness in the plastic region (above load

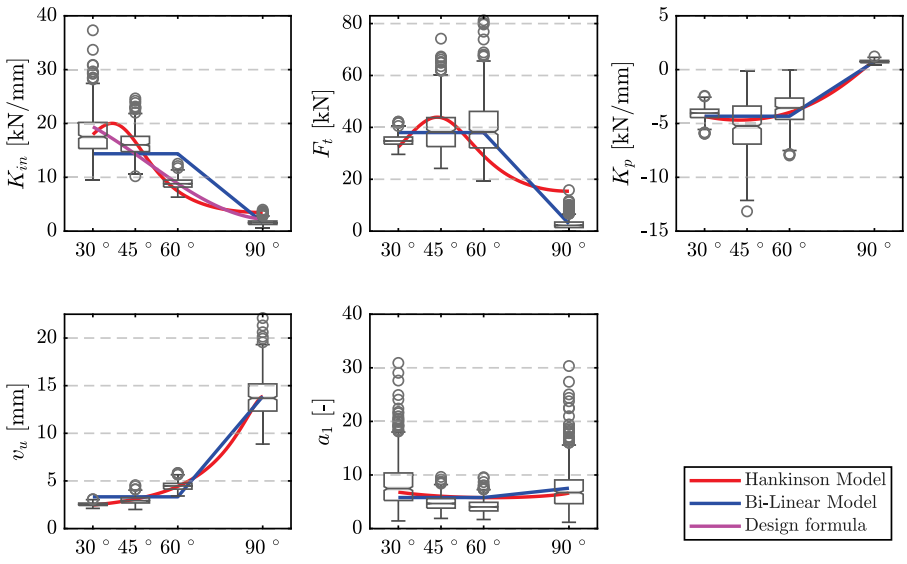

Fig. 12. Boxplot plots of Richard-Abbott regression parameter and fitting over the load-to-screw axis angle.

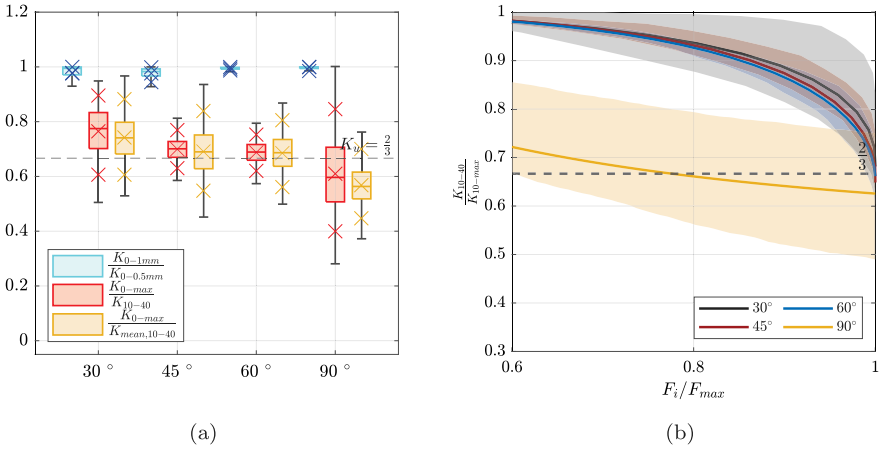

Fig. 13. (a): Stiffness ratios over the load-to-screw axis angle, (b): Evolution of the ratio in function of the load level in the joint.

levels larger than 2/3 of the design value of the load-carrying capacity) exhibits greater variability, with the ratio of 2/3 representing the average mean value across all load levels. For the joints with inclined screws, the ratio between K_{10-40}/K_{10-max} changes with the load level, ranging from 0 to 0.6. Consequently, it is challenging to establish a constant, load-independent ratio in this case.

5.3. Ductility

For each load-to-screw axis angle, both relative and absolute ductility were calculated using the following definitions:

$$D_{ab} = v_u - v_y \tag{15}$$

$$D_{rel} = \frac{v_u}{v_y} \tag{16}$$

where v_y is the displacement at the yielding point of the curve, v_u is the ultimate displacement, i.e. the displacement at failure. In this paper, v_y and v_u are computed based on indications contained in EN 12512 [36,48]. According to EN 12512 [36], the yielding point is found as the intersection between the initial stiffness K_{10-40} and the tangential stiffness to the graph with an inclination equal to $\frac{1}{6} \cdot K_{10-40}$. The intersection point is then projected onto the curve. The ultimate displacement v_u was taken as displacement at 80% of the load-carrying capacity, or as 30 mm, whichever occurs first.

Both the relative and absolute ductility are affected by variability, as shown by the (CoVs) in Fig. 14, for all the load-to-screw axis angles. Notably, the most significant differences occur between joints with screws that are laterally and axially loaded and those with screws that are laterally loaded only—the latter exhibiting a higher mean value of ductility.

6. Conclusions

The mechanical behaviour of steel-to-timber joints is characterized by complex load–displacement behaviour. In particular, the shape of the load-deformation curve and its variability are strongly influenced by the load-to-screw axis angle. However, the variability of the data in function of the load–displacement curve is scarcely investigated in the literature. An experimental investigation was conducted on steel-to-timber joints with laterally and laterally-axially loaded screws. First, an insight into the main parameters influencing the load–displacement curve was given. Then, 10 or 20 repetitions per configuration were performed, revealing how the variability of the data was affected by the load-to-screw axis angle. An empirical-probabilistic model was developed following 5 steps: regression of the curve based on the Richard-Abbott model, assignment of the probabilistic distribution,

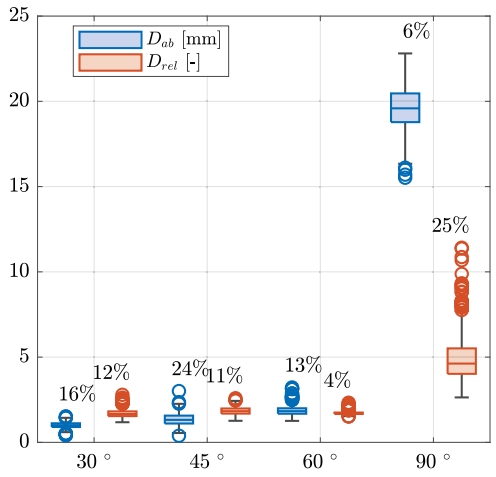

Fig. 14. Ductility ratios over load-to-screw axis angle. The values of ductility are calculated only for head-tear-off failure.

calculation of the correlation coefficients, and regression over the load-to-screw axis angle based on the bi-linear model. The main outcomes of the study are the following:

- Asymmetric test set-up can be a valid alternative to test joints with a single screw to isolate the fastener behaviour;
- Load–displacement curves of joints with screws frequently exhibit pronounced non-linearities due to factors such as varying fiction levels, torque, load-to-screw axis angle, and the presence of a washer, making the load–displacement curve exhibit complex shape. This highlighted the necessity of accounting the nonlinearities in the description of their mechanical behaviour;
- The Richard-Abbott model can be used to parametrize the load–displacement curve of joints with screws, representing the complexities, non-linearities and the variability of the load–displacement curve;
- Given the physical-based and analytical dependencies among the regression parameters of the Richard-Abbott model, the correlation coefficients must be considered to represent the variability of the load–displacement curves realistically;
- The bi-linear formula can represent the trend of the coefficient over the load-to-screw axis angle, but more data between the load-to-screw axis angle of 60° and 90° are needed to verify this trend;
- The ratio $\frac{K_{SLS}}{K_{ULS}}$ is affected by the load level at which the joint is utilized for joints with screws with a load-to-screw axis angle between 30° and 60° and it is affected by large variability for the joints with screws with a load-to-screw axis angle of 90°;
- The current deterministic definitions of K_{ULS} can be questioned for steel-to-timber joints with inclined and perpendicular screws, given the variability of load–displacement curves.
- Data-based definitions are recommended to represent the mechanical behaviour of joints in finite element analysis or reliability studies.

The findings exposed herein should be interpreted in light of several limitations concerning the extent of the experimental programme and, consequently, the empirical-probabilistic modelling:

- All the experimental tests were performed on joints containing a single screw. Therefore the impact of the number of screws on the load–displacement curve cannot be captured in the empirical-probabilistic model;
- The empirical-probabilistic model was developed varying only the load-to-screw axis angle. Other influential parameter: the diameter, the screw length, the testing loading rate and long-term effect were not varied. Therefore, the predictive capabilities of the model outside these testing conditions and with screws with different geometrical characteristic was not demonstrated.

These limitations do not undermine the qualitative insights into single fastener behaviour but constrain generalization. Future work should include multi-screw configurations, explore a wider range of screw diameters, and expand the test matrix to build a more robust empirical probabilistic model.

Moreover, a reliability-based analysis of structures is needed to clarify which definition of K_{ULS} is suitable for steel-to-timber joints with laterally and axially loaded screws.

CRediT authorship contribution statement

Dorotea Caprio: Writing – review & editing, Writing – original draft, Visualization, Validation, Software, Resources, Methodology, Investigation, Formal analysis, Data curation, Conceptualization. **Robert Jockwer:** Writing – review & editing, Supervision, Project administration, Methodology, Funding acquisition, Conceptualization.

Declaration of Generative AI and AI-assisted technologies in the writing process

During the preparation of this work, the authors occasionally used ChatGPT to improve the readability and grammar of some of the sentences. After using this tool, the authors reviewed and edited the content as needed and take full responsibility for the content of the published article.

Funding

This work was carried out within the project “RelyConnect — Reliable and high-performance timber structures with modern connections” (project number 2023-01603), funded by FORMAS, the Swedish research council for sustainable development, and was partly funded by Svensk Trä, the Swedish association of the timber industries, and TMF Swedish Federation of Wood and Furniture Industry (Träoch Möbelföretagen), Sweden is gratefully acknowledged. Würth is also acknowledged for providing the self-tapping screws and the washers used in the study.

Declaration of competing interest

The authors declare that they have no known competing financial interests or personal relationships that could have appeared to influence the work reported in this paper.

Data availability

Data will be made available on request.

References

[1] E. Acler, Nanyang Technological University sports hall – Singapore, in: Proceedings of the 23rd Internationales Holzbau-Forum, IHF, Garmisch-Partenkirchen, Germany, 2017.

[2] J. Rebhahn, M. Stenberg Ringnér, World of Volvo, Gothenburg - pushing the boundaries, in: Proc. of the 26th Internationales Holzbau-Forum IHF, Innsbruck, Austria, 2022.

[3] K.A. Malo, R.B. Abrahamsen, M.A. Bjertnæ s, Some structural design issues of the 14-storey timber framed building "Treet" in Norway, Eur. J. Wood Wood Prod. 74 (3) (2016) 407–424, http://dx.doi.org/10.1007/s00107-016-1022-5.

[4] EN 1995-1-1: Eurocode 5: Design of timber structures – Part 1-1: General and rules for buildings, European Committee for Sandardization, Bruxelles, Belgium, 2010.

[5] A. Ringhofer, R. Brandner, G. Schickhofer, Withdrawal resistance of self-tapping screws in unidirectional and orthogonal layered timber products, Mater. Struct. 48 (2015) 1435–1447, http://dx.doi.org/10.1617/s11527-013-0244-9.

[6] R. Brandner, A. Ringhofer, T. Reichinger, Performance of axially-loaded self-tapping screws in hardwood: Properties and design, Eng. Struct. 188 (2019) 677–699, http://dx.doi.org/10.1016/j.engstruct.2019.03.018.

[7] T. Claus, W. Seim, J. Küllmer, Force distribution in self-tapping screws: experimental investigations with fibre Bragg grating measurement screws, Eur. J. Wood Wood Prod. 80 (1) (2022) 183–197, http://dx.doi.org/10.1007/s00107-021-01740-z.

[8] T. Joyce, Y.H. Chui, Group effects in axially loaded self-tapping screw connections, Eng. Struct. 251 (2022) 113537, http://dx.doi.org/10.1016/j.engstruct.2021.113537.

[9] U. Mahlknecht, R. Brandner, Block shear failure mechanism of axially-loaded groups of screws, Eng. Struct. 183 (2019) 220–242, http://dx.doi.org/10.1016/j.engstruct.2018.12.057.

[10] Y. Steige, H.J. Blaß, Stiffness of axially loaded fully threaded screws, in: Proc. of the World Conference on Timber Engineering, WCTE, Seoul, Republic of Korea, 2018.

[11] M.A.H. Mirdad, A. Jucutan, R. Khan, J. Niederwestberg, Y.H. Chui, Embedment and withdrawal stiffness predictions of self-tapping screws in timber, Constr. Build. Mater. 345 (2022) 128394, http://dx.doi.org/10.1016/j.conbuildmat.2022.128394.

[12] M. Chybiński, K. Polus, Withdrawal strength of hexagon head wood screws in laminated veneer lumber, Eur. J. Wood Wood Prod. 80 (3) (2022) 541–553, http://dx.doi.org/10.1007/s00107-022-01797-4.

[13] D. Hoffmeyer, J. Munch-Andersen, Withdrawal capacity of screws in plywood and manufacturer dependencies, Eng. Struct. 321 (2024) 118973, http://dx.doi.org/10.1016/j.engstruct.2024.118973.

[14] M. Chybiński, Ł. Polus, Mechanical behaviour of aluminium–timber composite connections with screws and toothed plates, Materials 15 (2022) 68, http://dx.doi.org/10.3390/ma15010068.

[15] R. Tomasi, A. Crosatti, M. Piazza, Theoretical and experimental analysis of timber-to-timber joints connected with inclined screws, Constr. Build. Mater. 24 (2010) 1560–1571, http://dx.doi.org/10.1016/j.conbuildmat.2010.03.007.

[16] H. Krenn, G. Schickhofer, Joints with inclined screws and steel plates as outer members, in: Proceedings of CIB-W18 Meeting 42 (42-7-2), Dübendorf, Switzerland, 2009.

[17] R. Jockwer, R. Steiger, A. Frangi, Fully threaded self-tapping screws subjected to combined axial and lateral loading with different load to grain angles, in: S. Aicher, H.-W. Reinhardt, H. Garrecht (Eds.), Materials and Joints in Timber Structures, in: RILEM Bookseries, vol. 9, Springer, Dordrecht, 2014, pp. 265–272.

[18] C. Binck, A. Cao, A. Frangi, Lateral stiffening systems for tall timber buildings–tube-in-tube systems, Wood Mater. Sci. Eng. (2022) 1–8, http://dx.doi.org/10.1080/17480272.2022.2086066.

[19] H.J. Blaß, I. Bejtka, T. Uibel, Tragfähigkeit von Verbindungen mit selbstbohrenden Holzschrauben mit Vollgewinde, Vol. 4, KIT Scientific Publishing Karlsruhe, Germany, 2006.

[20] Y. De Santis, M. Fragiacomo, Timber-to-timber and steel-to-timber screw connections: Derivation of the slip modulus via beam on elastic foundation model, Eng. Struct. 244 (2021) 112798, http://dx.doi.org/10.1016/j.engstruct.2021.112798.

[21] Y. De Santis, A. Aloisio, D.P. Pasca, I. Gavrić, M. Fragiacomo, Mechanical characterization of soundproofed inclined screws connections, Constr. Build. Mater. 412 (2024) http://dx.doi.org/10.1016/j.conbuildmat.2023.134641.

[22] A. Jorissen, Double-Shear Timber Connections with Dowel-Type Fasteners (Ph.D. thesis), Delft University of Technology, Delft, The Netherlands, 1998.

[23] G. Flatscher, Evaluation and Approximation of Timber Connection Properties for Displacement-Based Analysis of CLT Wall Systems (Ph.D. thesis), Graz University of Technology, Graz, Austria, 2017.

[24] D. Caprio, R. Jockwer, Regression models for the description of the behaviour of modern timber joints, Build. 13 (11) (2023) http://dx.doi.org/10.3390/buildings13112693.

[25] M. Schweigler, T.K. Bader, G. Hochreiner, R. Lemaî tre, Parameterization equations for the nonlinear connection slip applied to the anisotropic embedment behavior of wood, Compos. Part B: Eng. 142 (2018) 142–158, http://dx.doi.org/10.1016/j.compositesb.2018.01.003.

[26] R. Brandner, A. Ringhofer, M. Grabner, Probabilistic models for the withdrawal behavior of single self-tapping screws in the narrow face of cross laminated timber (CLT), Eur. J. Wood Wood Prod. 76 (1) (2018) 13–30, http://dx.doi.org/10.1007/s00107-017-1226-3.

[27] P. Glos, Zur Bestimmung des Festigkeitsverhaltens von Brettschichtholz bei Druckbeanspruchung aus Werkstoff-und Einwirkungskenngrößen (Ph.D. thesis), Technische Universität München, Munich, Germany, 1978.

[28] C. Bedon, M. Sciomenta, M. Fragiacomo, Mechanical characterization of timber-to-timber composite (TTC) joints with self-tapping screws in a standard push-out setup, Appl. Sci. 10 (18) (2020) 6534, http://dx.doi.org/10.3390/app10186534, Number: 18 Publisher: Multidisciplinary Digital Publishing Institute.

[29] T. Bader, J.-F. Bocquet, M. Schweigler, R. Lemaitre, Numerical Modeling of the Load Distribution in Multiple Fastener Connections., 2018, pp. 221–239.

[30] M. Schweigler, T. Bader, G. Hochreiner, Engineering modeling of semi-rigid joints with dowel-type fasteners for nonlinear analysis of timber structures, Eng. Struct. 171 (2018) 123–139, http://dx.doi.org/10.1016/j.engstruct.2018.05.063.

[31] EN 14080: Timber Structures - Glued Laminated Timber and Glued Solid Timber, European Committee for Standardization CEN, Bruxelles, Belgium, 2013.

[32] EN 13183-1: Hygrothermal Performance of Building Materials and Products—Determination Of Moisture Content—Part 1: Oven-dry Method, European Committee for Standardization (CEN), 2002.

[33] ETA-11/0190 Self-Tapping Screws for Use in Timber Constructions, EOTA, 2018.

[34] ISO 6892-1: Metallic materials - tensile testing - part 1: Method of test at room temperature, International Organization for Standardization, 2019.

[35] EN 1990 - Eurocode 0: Basis of Structural Design, European Committee for Standardization CEN, 2002.

[36] EN 12512 - Timber structures - Test methods - Cyclic Testing of Joints Made with Mechanical Fasteners., Standard, European Committee for Standardization CEN, Bruxelles, Belgium, 2002, Type.

[37] JCSS, Probabilistic Model Code, Joint Committee on Structural Safety, www.jcss-lc.org, 2006.

[38] G. GmbH., Aramis adjustable. URL https://www.gom.com/metrology-systems/aramis/aramis-adjustable.html.

[39] EN 14358: Timber Structures - Calculation and Verification of Characteristic Values, European Committee for Standardization CEN, 2016.

[40] I. Smith, G. Foliente, Load and resistance factor design of timber joints: International practice and future direction, J. Struct. Eng. 128 (1) (2002) 48–59, http://dx.doi.org/10.1061/(ASCE)0733-9445(2002)128:1(48), Publisher: American Society of Civil Engineers.

[41] ISO 8503-1: Preparation of Steel Substrates Before Application of Paints and Related Products — Surface Roughness Characteristics of Blast-Cleaned Steel Substrates, International Organization for Standardization.

[42] D. Caprio, R. Jockwer, A. Ringhofer, Parametrization of the non-linear behaviour of timber joints with self-tapping screws, in: Proc. of Meeting No. 11 of the International Network on Timber Engineering Research INTER, Paper No. 57-7-7, Padua, Italy, 2024.

[43] R. Hankinson, Investigation of crushing strength of spruce at varying angles of grain, Air Serv. Inf. Circ. 3 (259) (1921) 130.

[44] prEN 1995-1-1: Eurocode 5 - Design of Timber Structures — Part 1-1: General Rules and Rules for Buildings., European Committee for Standardization CEN, Bruxelles, Belgium, 2023.

[45] J. Ehlbeck, H. Werner, Untersuchungen über die Tragfähigkeit von Stabdübelverbindungen, Holz Als Roh- Und Werkst. 46 (8) (1988) 281–288, http://dx.doi.org/10.1007/BF02615055.

[46] J.J. Mack, The strength and stiffness of nailed joints under short-duration loading, Division of Forest Products technological paper, Commonwealth Scientific and Industrial Research Organization, Australia, Melbourne, Australia, 1966.

[47] EN 1993-1-1: Eurocode 3: Design of Steel Structures - Part 1-1: General Rules and Rules for Buildings, European Committee for Sandardization CEN, Bruxelles, Belgium, 2004.

[48] R. Jockwer, D. Caprio, A. Jorissen, Evaluation of parameters influencing the load-deformation behaviour of connections with laterally loaded dowel-type fasteners, Wood Mater. Sci. Eng. (2021) 1–14, http://dx.doi.org/10.1080/17480272.2021.1955297.